Temperature and magnetic field dependence of spin-ice correlations in the pyrochlore magnet Tb$_2$Ti$_2$O$_7$

K. Fritsch,[1,*] E. Kermarrec,[1] K. A. Ross,[2,3] Y. Qiu,[3,4] J. R. D. Copley,[3] D. Pomaranski,[5,6] J. B. Kycia,[5,6]
H. A. Dabkowska,[7] and B. D. Gaulin[1,7,8]

[1]*Department of Physics and Astronomy, McMaster University, Hamilton, Ontario L8S 4M1, Canada*
[2]*Institute for Quantum Matter and Department of Physics and Astronomy, Johns Hopkins University, Baltimore, Maryland 21218, USA*
[3]*NIST Center for Neutron Research, NIST, Gaithersburg, Maryland 20899-8102, USA*
[4]*Department of Materials Science and Engineering, University of Maryland, College Park, Maryland 20742, USA*
[5]*Department of Physics and Astronomy and Guelph-Waterloo Physics Institute, University of Waterloo, Waterloo, Ontario N2L 3G1, Canada*
[6]*Institute for Quantum Computing, University of Waterloo, Waterloo, Ontario N2L 3G1, Canada*
[7]*Brockhouse Institute for Materials Research, Hamilton, Ontario L8S 4M1, Canada*
[8]*Canadian Institute for Advanced Research, 180 Dundas Street West, Toronto, Ontario M5G 1Z8, Canada*

We present a parametric study of the diffuse magnetic scattering at $(\frac{1}{2},\frac{1}{2},\frac{1}{2})$ positions in reciprocal space, ascribed to a frozen antiferromagnetic spin ice state in single-crystalline Tb$_2$Ti$_2$O$_7$. Our high-resolution neutron scattering measurements show that the elastic (-0.02 meV $< E < 0.02$ meV) $(\frac{1}{2},\frac{1}{2},\frac{1}{2})$ scattering develops strongly below $\approx$275 mK, and correlates with the opening of a spin gap of $\approx$0.06 to 0.08 meV over most of the Brillouin zone. The nature of the transition at 275 mK has many characteristics of spin glass behavior, consistent with ac-susceptibility measurements. The application of a magnetic field of 0.075 T applied along the [1$\bar{1}$0] direction destroys the $(\frac{1}{2},\frac{1}{2},\frac{1}{2})$ elastic scattering, revealing the fragility of this short-range ordered ground state. We construct a refined H-T phase diagram for Tb$_2$Ti$_2$O$_7$ and [1$\bar{1}$0] fields which incorporates this frozen spin ice regime and the antiferromagnetic long-range order previously known to be induced in relatively large fields. Specific heat measurements on the same crystal reveal a sharp anomaly at $T_c \approx 450$ mK and no indication of a transition near $\approx$275 mK. We conclude that the higher temperature specific heat peak is not related to the magnetic ordering but is likely a signal of other, nonmagnetic dipole correlations.

I. INTRODUCTION

The search for experimental realizations of quantum spin liquid and quantum spin ice (QSI) states is of great current interest [1,2] due to the potential for exotic physics within these systems. Geometrically frustrated magnetic materials are central to the discovery of such exotic states [3]. Besides materials based on quasi-two-dimensional lattices such as herbertsmithite [4–6] or the organic spin liquid candidate κ-(BEDT-TTF)$_2$Cu$_2$(CN)$_3$ [7,8], the three-dimensional pyrochlore lattice consisting of networks of corner-sharing tetrahedra has been the focus of significant and sustained research efforts [1,2,9–11]. The family of rare-earth-based titanate pyrochlores has played a prominent role in these studies as many members of this family can be grown as large and pristine single crystals [12–15]. Within this family, Tb$_2$Ti$_2$O$_7$ stands out as perhaps the least well understood, despite having been studied in this context for well over a decade [16]. In this material, the Tb^{3+} magnetic moments that decorate the pyrochlore lattice are expected to display Ising-like easy axis anisotropy with spins pointing along the local $\langle 111 \rangle$ axes, either into or out of the tetrahedra, as a consequence of their crystal field (CF) doublet ground state [17–19]. Based on a negative Curie-Weiss temperature ($\Theta_{CW} \approx -14$ K) and this Ising-like anisotropy, mean-field theory predicts the classical ground state of Tb$_2$Ti$_2$O$_7$ to not be frustrated, and Tb$_2$Ti$_2$O$_7$ is, on the basis of Monte Carlo simulations [20], expected to order into an antiferromagnetic (AF) $\mathbf{Q} = 0$ Néel ordered state around $\approx$1 K [17]. Yet, this material fails to exhibit conventional long-range order (LRO) down to at least 50 mK as shown in very early studies by Gardner *et al.* [16,21].

This puzzle has motivated two vigorously debated [22–25] theoretical scenarios to account for Tb$_2$Ti$_2$O$_7$'s disordered ground state: a quantum spin ice (QSI) scenario [22,23,26] and a nonmagnetic singlet ground state [27]. The QSI proposal introduces quantum dynamics to the problem through virtual fluctuations of the Tb^{3+} ions between their ground state and excited CF doublets. These quantum fluctuations reposition Tb$_2$Ti$_2$O$_7$ into the nearby spin ice regime within a generalized phase diagram appropriate to Ising-like pyrochlore magnets [20]. This quantum spin ice state is somewhat different from the one recently described by Benton *et al.* [28], in which quantum fluctuations are introduced via tunneling between spin ice configurations. The nonmagnetic singlet scenario assumes a splitting of the accidental CF doublet ground state of the Tb^{3+} ions ($J = 6$, non-Kramers) into two nonmagnetic singlets through a Jahn-Teller-like symmetry lowering of the CF environment, thus producing a nonmagnetic ground state. The latter scenario implies a noncubic structure at low but finite temperatures in Tb$_2$Ti$_2$O$_7$. To date, evidence for such a static structural distortion is lacking at all but very large magnetic fields [29,30].

More recently, evidence for the presence of strong magnetoelastic coupling has been reported in inelastic neutron

---

*Present address: Helmholtz-Zentrum Berlin für Materialien und Energie, D-14109 Berlin, Germany; katharina.fritsch@helmholtz-berlin.de

scattering measurements [31,32] with the observation of a magnetoelastic mode, resulting from the hybridization of the first excited crystal field level and transverse acoustic phonons. This mode appears to be gapped below ≈ 1 meV, and as such exists on a rather high energy scale of ≈ 11 K. Its discovery reaffirms the importance of the spin-lattice coupling in $Tb_2Ti_2O_7$ [33,34].

Other recent experiments on $Tb_2Ti_2O_7$ have revealed features associated with the QSI state, most notably pinch-point-like diffuse scattering [32,35–37] indicative of Coulombic correlations, and signs of a magnetization plateau for magnetic fields along [111] theoretically proposed by Molavian *et al.* [26], although the existence of this latter feature remains under debate. Several groups reported anomalies in the ac susceptibility below 100 mK (down to 43 mK) [38–40], but with an overall monotonic decrease of the susceptibility versus field, therefore lacking a true inflection in $M(\mu_0 H)$ such that the presence of a plateau was clear. On the other hand, Yin *et al.* [41] performed ac-susceptibility measurements down to 16 mK, with a slow field-sweep rate, and found an additional anomaly at $\mu_0 H = 0.59$ T, which does correspond to an inflection point in $M(\mu_0 H)$, and from which they inferred the existence of a magnetization plateau occurring between 0.063 T and 0.59 T. The extremely low temperature achieved in this experiment seems to have been key to the observation of this feature [38–40,42,43]. According to the single-tetrahedron model previously mentioned [26], the application of a field along [111] preserves the QSI ground state until, for $H > H^*$, a partially spin polarized state (or quantum kagome ice) is stabilized, characterized by a plateau in $M(\mu_0 H)$. The experimental observation of Yin *et al.* supports this scenario and they interpret the low-field, low-T state of their phase diagram ($\mu_0 H < 0.067$ T, $T < 140$ mK) to be the QSI state. Here, we investigate this low-field, low-T state via inelastic neutron scattering.

Our recent high-resolution neutron scattering measurements [37] on single-crystalline $Tb_2Ti_2O_7$ at 70 mK have revealed short-range spin ice correlations at $(\frac{1}{2},\frac{1}{2},\frac{1}{2})$ wave vectors which can be ascribed to a short-range antiferromagnetically ordered spin ice state with spin canting at an angle of $\approx 12°$ from the local $\langle 111 \rangle$ axes. These static correlations observed in the elastic scattering channel were shown to be very sensitive to both applied magnetic field and temperature, although parametric studies of the field and temperature dependence of this scattering were not performed. The static $(\frac{1}{2},\frac{1}{2},\frac{1}{2})$ correlations were separated from low-lying inelastic magnetic excitations by a spin gap of ≈ 0.06 to 0.08 meV. Other neutron studies also observed diffuse scattering intensity at $(\frac{1}{2},\frac{1}{2},\frac{1}{2})$ positions; however, these studies did not relate the scattering to a short-range antiferromagnetically ordered spin ice state [35,36]. A subsequent study of nonstoichiometric $Tb_{2+x}Ti_{2-x}O_{7+y}$ by Taniguchi *et al.* [44] also observed the appearance of a $(\frac{1}{2},\frac{1}{2},\frac{1}{2})$ Bragg-like peak associated with quasi-long-range order at low temperatures in a polycrystalline sample which was lightly "stuffed," $Tb_{2+x}Ti_{2-x}O_{7+y}$ ($x = 0.005$).

In this paper, we report a detailed study of the temperature and field dependence of the previously observed elastic $(\frac{1}{2},\frac{1}{2},\frac{1}{2})$ and associated low-lying inelastic scattering in $Tb_2Ti_2O_7$. We show that the elastic scattering appears upon lowering the temperature below ≈ 275 mK and that

its appearance correlates with the opening of a spin gap within the low-lying magnetic spectral weight over most of the Brillouin zone. This magnetic spectral weight appears to soften somewhat at the "quasi"-ordering wave vector $(\frac{1}{2},\frac{1}{2},\frac{1}{2})$ at the lowest temperature measured, $T = 80$ mK. The application of a magnetic field along $[1\bar{1}0]$ leads to a destruction of the short-range ordered ground state by $\mu_0 H = 0.075$ T. We construct a new H-T phase diagram for $Tb_2Ti_2O_7$ in a $[1\bar{1}0]$ magnetic field, which encompasses both this new frozen spin ice state at very low fields and temperature, and the previously known long-range ordered antiferromagnetic state which exists at relatively high fields and over a much larger range of temperatures.

II. EXPERIMENTAL DETAILS

The single-crystal sample of $Tb_2Ti_2O_7$ used for the neutron scattering measurements we present here is the same sample used in earlier studies [37,45] and was grown using the optical floating zone technique at McMaster University [46,47]. High-resolution x-ray diffraction measurements on a powder sample produced from a small piece of this single crystal determined the cubic lattice parameter a to be 10.1568(6) Å at room temperature, as compared with 10.1536(1) Å from nominally stoichiometric $Tb_2Ti_2O_7$ [44], and 10.155 288(1) Å from the recent work by Fennell *et al.* [31].

Time-of-flight neutron scattering measurements were performed using the disk-chopper spectrometer DCS [48] at the NIST Center for Neutron Research. Two different incident energies were employed; for lower energy resolution measurements we used $E_i = 3.27$ meV, giving an energy resolution of 0.1 meV, while the higher energy resolution measurements we report used $E_i = 1.28$ meV with a resulting resolution of 0.02 meV. The sample was carefully aligned with the $[1\bar{1}0]$ direction vertical to within $0.5°$, such that the (H,H,L) plane was coincident with the horizontal scattering plane. Measurements were performed in a temperature range of 80 mK $< T \lesssim$ 650 mK and at magnetic fields $\leqslant 0.2$ T.

Specific heat measurements were performed with a ^{3}He/^{4}He dilution refrigerator at the University of Waterloo. The crystal used for neutron scattering measurements was cut and sectioned into a 33.8 mg mass with dimensions 2.6 $\times$ 2.6 $\times$ 1.3 mm^3 and this smaller single crystal was used in the heat capacity study. The relaxation method was employed with a thermal weak link of manganin wire, with conductance 5.0×10^{-7} J/K/s at 0.80 K. The resulting time constant was greater than 600 s at the highest temperature measured. The average step size for the relaxation measurement was 3.5% of the nominal temperature, with a minimum equilibration time window of five times the thermal relaxation constant.

III. MAGNETIC FIELD DEPENDENCE

Figure 1 shows a series of elastic scattering maps in the (H,H,L) plane for different magnetic fields applied along $[1\bar{1}0]$ in panels (a) through (e). Here, elastic scattering integrates over -0.1 meV $< E < 0.1$ meV in energy. Figure 1(f) shows a cut of this elastic scattering, along the [111] high-symmetry direction covering the $(-0.5, -0.5, 1.5)$, $(0.5, 0.5, 2.5)$ as well as the $(0,0,2)$ and $(1,1,3)$ Bragg positions, as indicated by the yellow dashed line in Fig. 1(e). As the applied magnetic field

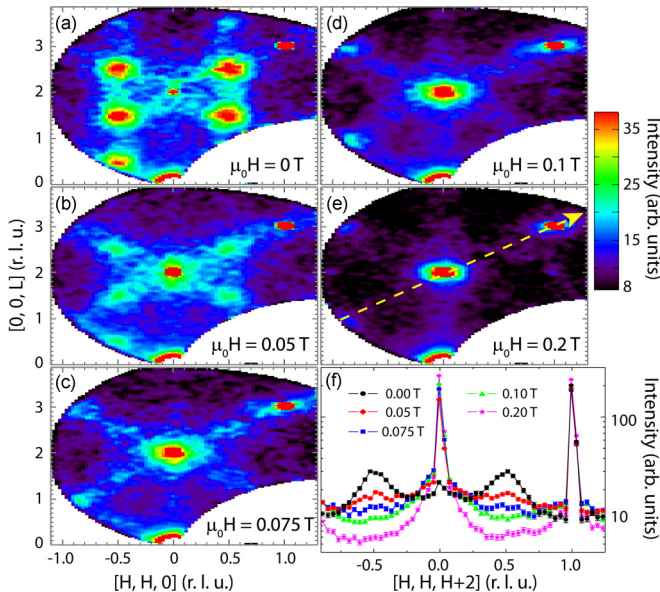FIG. 1. (Color online) Elastic neutron scattering data within the (H,H,L) plane of $Tb_2Ti_2O_7$ at $T = 80$ mK for different values of applied magnetic field ($H \parallel [1\bar{1}0]$). The energy is integrated over $[-0.1,0.1]$ meV. Panels (a) through (e) show the evolution of the elastic scattering for an applied magnetic field of 0, 0.05, 0.075, 0.1, and 0.2 T, respectively. Panel (f) shows the magnetic field dependence of the elastic scattering along the [111] direction cutting through the (0,0,2) Bragg position as indicated by the yellow arrow in panel (e). The $(\frac{1}{2},\frac{1}{2},\frac{1}{2})$ peaks vanish around $\mu_0 H \approx 0.075$ T. All data have an empty can background subtracted. The error bars are $\pm 1\sigma$.

FIG. 2. (Color online) Integrated elastic scattering at the $(\frac{1}{2},\frac{1}{2},\frac{1}{2})$ and (0,0,2) positions as a function of magnetic field. The $(\frac{1}{2},\frac{1}{2},\frac{1}{2})$ scattering gets clearly suppressed at ≈ 0.075 T. The inset shows a color contour map of the diffuse elastic scattering around the (0,0,2) Bragg peak made of line scans along [H,H,2] on a logarithmic intensity scale. The binning range for this cut was $L = [1.9,2.1]$ r.l.u.. The intensity of the resolution-limited weak elastic scattering at (0,0,2) in zero field has been subtracted. Diffuse scattering from the $(\frac{1}{2},\frac{1}{2},\frac{1}{2})$ positions is seen to extend out to (0.5,0.5,2) and $(-0.5, -0.5,2)$ below 0.075 T; above this field, the diffuse scattering increases in intensity and narrows considerably at the (0,0,2) position. An empty can background subtraction and correction for detector efficiency were performed for all data shown. Error bars are $\pm 1\sigma$.

is increased to 0.05 T, the previously observed strong diffuse scattering at the $(\frac{1}{2},\frac{1}{2},\frac{1}{2})$ positions in zero field [panel (a)] gets suppressed substantially [panel (b)] and is much reduced by 0.075 T [panel (c)].

Simultaneous to the suppression of the $(\frac{1}{2},\frac{1}{2},\frac{1}{2})$ diffuse scattering intensity in fields up to 0.075 T, we observe a strong buildup in magnetic elastic intensity at the structurally forbidden (0,0,2) Bragg peak. As the field is increased further [panels (d) and (e)], most of the remaining diffuse scattering condenses into the Bragg position at (0,0,2). The intensity scale is linear for Figs. 1(a)–1(e). In contrast, the cut along the [111] direction through (0,0,2) in Fig. 1(f) is plotted on a logarithmic intensity scale. Note that the highest applied field here, 0.2 T, is still far below the critical $[1\bar{1}0]$ field ≈ 2 T, above which $Tb_2Ti_2O_7$ is found in a field-induced antiferromagnetic long-range ordered state, characterized by the appearance of resolution-limited spin waves and a strong (1,1,2) magnetic Bragg peak [45].

A further feature in the elastic scattering maps is the appearance of weak rods of scattering along both the $\langle 00L \rangle$ and $\langle 111 \rangle$ directions that can be identified as evidence for significant anisotropic exchange in $Tb_2Ti_2O_7$ [35]. Rods of magnetic scattering have been identified in other rare-earth titanate pyrochlores, such as $Yb_2Ti_2O_7$ [49], where anisotropic exchange is well established [13,50,51]. Anisotropic exchange in $Tb_2Ti_2O_7$ has recently been investigated in papers by Bonville *et al.* [25] and by Curnoe [52], the latter of which related an effective $S = 1/2$ spin Hamiltonian to
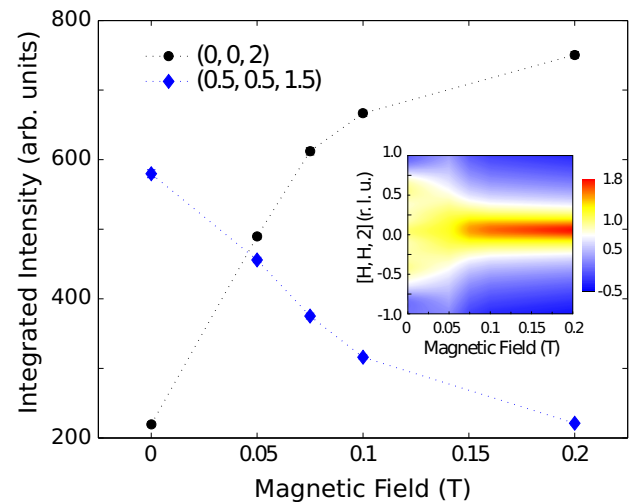
diffuse magnetic neutron scattering. Recent work by Bonville *et al.* [53] invoking a dynamic Jahn-Teller effect based on observations of magnetoelastic excitations coupling the crystal field excitations with acoustic phonon modes [31,32] can also successfully model the diffuse rods of scattering. However, such a scenario is not compatible with static magnetic correlations or with quasielastic scattering at very low temperature.

One can integrate up the elastic scattering data in a relatively small region around the $(\frac{1}{2},\frac{1}{2},\frac{1}{2})$ or (0,0,2) positions in reciprocal space, and look at their explicit $[1\bar{1}0]$ magnetic field dependence. This is what is shown in Fig. 2, with relatively small integration ranges of ± 0.2 r.l.u. in [H,H,H], and ± 0.15 r.l.u. perpendicular to [H,H,H] for $(\frac{1}{2},\frac{1}{2},\frac{1}{2})$, and ± 0.1 r.l.u. in [H,H,H] and ± 0.15 r.l.u. perpendicular to [H,H,H] for (0,0,2). We identify the inflection point in the field dependence of the $(\frac{1}{2},\frac{1}{2},\frac{1}{2})$ intensity near $\mu_0 H \approx 0.075$ T, as well as the leveling off of the (0,0,2) elastic intensity for fields beyond 0.075 T with the $T \approx 0$ phase boundary to the frozen, antiferromagnetic spin ice state in $Tb_2Ti_2O_7$. The inset to Fig. 2 shows a color map of the diffuse elastic scattering around the (0,0,2) position. This color map is made of a series of scans along [H,H,2], integrating over L= [1.9,2.1] r.l.u.. The resolution-limited weak scattering at (0,0,2) in zero magnetic field has been fitted and removed from the scattered intensity shown in this inset. As evident from this map and consistent with the integrated elastic intensity shown in Fig. 2, strong diffuse scattering at the $(\frac{1}{2},\frac{1}{2},\frac{1}{2})$ positions is present below $\mu_0 H = 0.075$ T, and this

extends across these [H,H,2] scans, that is to (0.5,0.5,2) and (−0.5, −0.5,2). For fields above $\mu_0 H = 0.075$ T, this diffuse scattering collapses into the (0,0,2) position.

The field dependence of the elastic magnetic scattering, and in particular the rapid fall-off of the $(\frac{1}{2},\frac{1}{2},\frac{1}{2})$ frozen spin ice elastic scattering near 0.075 T, is in qualitative agreement with recent work by Yin *et al.* [41]. They have proposed a low-temperature low-field phase diagram for $Tb_2Ti_2O_7$ based on magnetization and ac-susceptibility data. These measurements reveal two magnetic phases, the first one of which appears below 140 mK and for fields $\mu_0 H < 0.067$ T, while another phase is found at very low temperatures $T < 40$ mK and higher fields $0.067 < \mu_0 H < 0.6$ T. From the observation of a weak magnetization plateau in the presence of a [111] magnetic field, theoretically predicted by Molavian *et al.* [26], these authors conclude that a quantum kagome spin ice state exists at higher fields, with a QSI state at low and zero magnetic fields. Although these measurements by Yin *et al.* [41] were performed in a [111] applied magnetic field, we note that anisotropy in the magnetization of $Tb_2Ti_2O_7$ is only observed for field strengths exceeding $\gtrsim 0.3$ T [43], well above the range of applied field strengths which we report here in our neutron scattering measurements. For that reason, and as can be seen from the temperature dependence of the elastic scattering reported below, we consider the phase diagram presented in Ref. [41] to be germane to our findings.

IV. TEMPERATURE DEPENDENCE

The temperature dependence of the integrated elastic intensity of the $(\frac{1}{2},\frac{1}{2},\frac{1}{2})$ peaks in zero field is presented in Fig. 3. We determined the elastic integrated intensity (−0.1 meV $< E <$ 0.1 meV) at the four $(\frac{1}{2},\frac{1}{2},\frac{1}{2})$ positions in our field of view in Fig. 3(a) and average the integrated intensities at each temperature. The corresponding background signal for each T was obtained by integrating over a region of low intensity in reciprocal space around (1,1,2). This background term was subsequently subtracted from the averaged $(\frac{1}{2},\frac{1}{2},\frac{1}{2})$ integrated elastic intensity.

The results of these integrations are shown in Fig. 3(b) for individual heating and cooling runs labeled in the order of the measurements. Two prominent features become apparent in Fig. 3. First, the temperature dependence of the $(\frac{1}{2},\frac{1}{2},\frac{1}{2})$ peaks behaves in an order-parameter-like fashion with a distinctive drop in integrated intensity around 275 mK. Second, the ground state below 275 mK has some history dependence to it, with the elastic $(\frac{1}{2},\frac{1}{2},\frac{1}{2})$ peak intensity variable from one thermal history to the next. History dependence is a common feature of spin glass or frozen states [56,57]. We first discuss the second observation. Data points were collected in three temperature sweeps: heating A, cooling B, and heating B. Representative elastic reciprocal space maps for the two runs obtained during heating are shown in Fig. 3(a) for the low-temperature short-range ordered ground state (80 mK or 100 mK) and for the higher temperature disordered state (400 mK or 600 mK, respectively). We observe that the absolute intensity of the $(\frac{1}{2},\frac{1}{2},\frac{1}{2})$ elastic peaks in the second heating run is a factor of ∼2 smaller, and that the overall diffuse elastic scattering background is somewhat larger compared to the first heating run. This indicates that a complex freezing
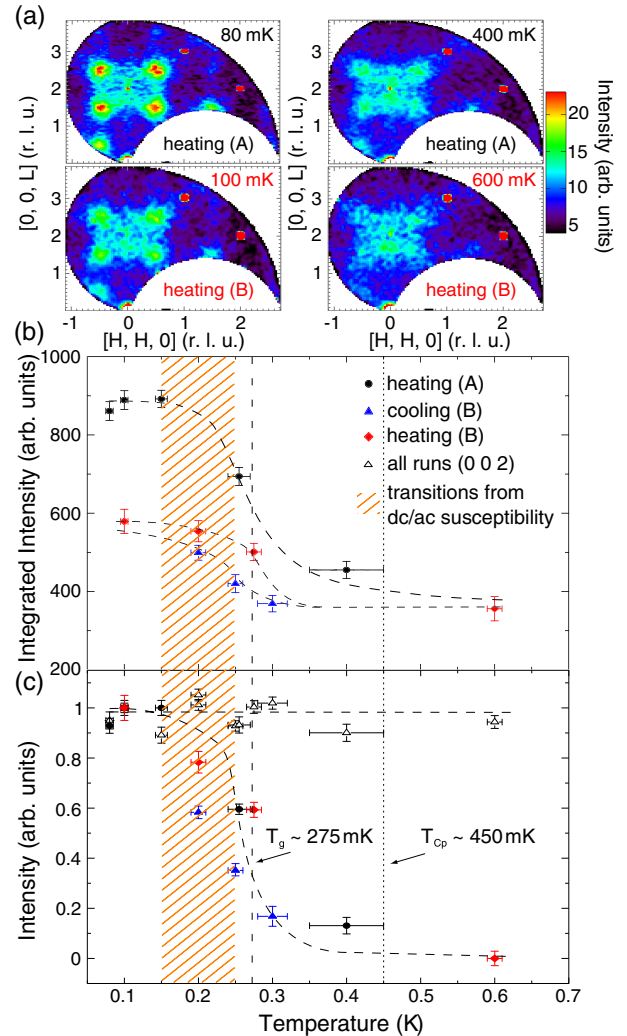

FIG. 3. (Color online) Temperature dependence of the elastic $(\frac{1}{2},\frac{1}{2},\frac{1}{2})$ scattering in zero field. The integrated elastic scattering intensity (−0.1 meV $< E <$ 0.1 meV, H = ±[0.4,0.6] r.l.u., L = [1.4,1.6] and L = [2.4,2.6] r.l.u.) at the four $(\frac{1}{2},\frac{1}{2},\frac{1}{2})$-like positions is presented as a function of temperature for different heating and cooling cycles in panel (b). See text for details. Representative reciprocal space maps for the two heating cycles are shown in panel (a). Panel (c) shows the integrated intensity from (b) scaled to the difference between the low-temperature phase at 100 mK and the high-temperature phase at 600 mK (heating B) or 400 mK (heating A), placing the transition below which $(\frac{1}{2},\frac{1}{2},\frac{1}{2})$ peaks appear at a temperature of ≈275 mK. In addition, the temperature dependence of the elastic (0,0,2) scattering, normalized to the intensity at the lowest temperatures, is shown on the same plot, indicating no obvious temperature dependence. Various reports of this glassy transition from ac-susceptibility measurements [21,38,54,55] are encompassed by the hatched area. The specific heat anomaly found for our crystal at $T_{Cp} \approx 450$ mK is indicated by a dotted vertical line. This anomaly appears at considerably higher temperature than the onset of the short-range magnetic ordering. Dashed lines serve as guides to the eyes.

process with several metastable states is likely at play at low temperatures. This is not so surprising, as the $(\frac{1}{2},\frac{1}{2},\frac{1}{2})$ elastic scattering does not correspond to long-range order, but
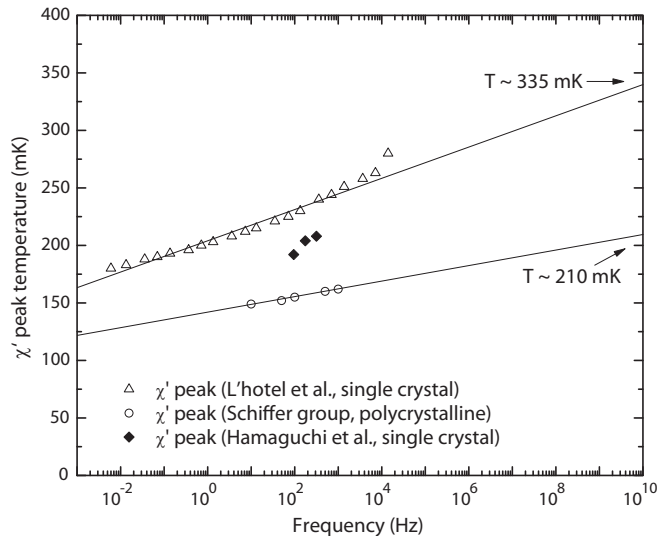
FIG. 4. Shift of the ac-susceptibility peaks per decade frequency for polycrystal and single crystalline samples from different groups [38,54,58]. For these measurements, the slope $\frac{\Delta T}{T\Delta(\log T)} < 0.1$, consistent with expectations for insulating spin glasses [56]. The extrapolation of the ac-susceptibility peak to frequencies on the order of 10^{10} Hz ≈ 0.04 meV, at which our measurements probe the system, shows that the expected transition occurs between 210 and 335 mK. The transition temperature we determine falls right within that range and is thus consistent with these measurements.

FIG. 5. (Color online) H-T phase diagram for $Tb_2Ti_2O_7$ in $[1\bar{1}0]$ magnetic field extracted from neutron scattering measurements in the low-field and low-temperature region presented in this work and from high-field and higher-temperature measurements by Rule *et al.* [45]. The magnetic phase transitions measured by Yin *et al.* [41] from ac susceptibility with fields along [111] are also shown.

rather is known to be characterized by a relatively short and isotropic correlation length of ≈ 8 Å, again typical of spin glass behavior. Despite this, a common feature in all three heating and cooling runs is the appearance of the $(\frac{1}{2},\frac{1}{2},\frac{1}{2})$ peaks below 275 mK. To make that point, we scaled and normalized the integrated elastic intensities at $(\frac{1}{2},\frac{1}{2},\frac{1}{2})$ from Fig. 3(b) to the difference in intensity between the low-temperature state at 100 mK or below and that of the high-temperature state (400 mK or 600 mK, respectively). The result is shown in Fig. 3(c), which shows a glass-like transition to occur around ≈ 275 mK, independent of the detailed history. We also note here that, in contrast to the elastic scattering at $(\frac{1}{2},\frac{1}{2},\frac{1}{2})$, the elastic scattering at $(0,0,2)$ does not show any significant temperature dependence as shown in Fig. 3(c).

The spin-glass-like transition as measured with the $(\frac{1}{2},\frac{1}{2},\frac{1}{2})$ elastic magnetic scattering is consistent with that observed by several groups using dc- [59] and ac-susceptibility measurements [21,38,54,58]. These data are summarized in Fig. 4, and peaks found in χ', the real part of the ac susceptibility, lie in the temperature range ≈ 150 to 250 mK. This temperature regime is indicated with an orange hatched area in Figs. 3(b) and 3(c), so that the results from elastic neutron scattering and ac susceptibility can be compared. As neutron scattering measurements are performed at relatively high frequencies compared with ac susceptibility, it is expected that neutron scattering measures spin freezing associated with spin glass transitions at higher temperatures than are observed in ac susceptibility. This is illustrated in Fig. 4, in which we show the linearly extrapolated peak shift per decade frequency, a phenomenological parameter used to describe the temperature dependence of the χ' peak in spin glasses as a function
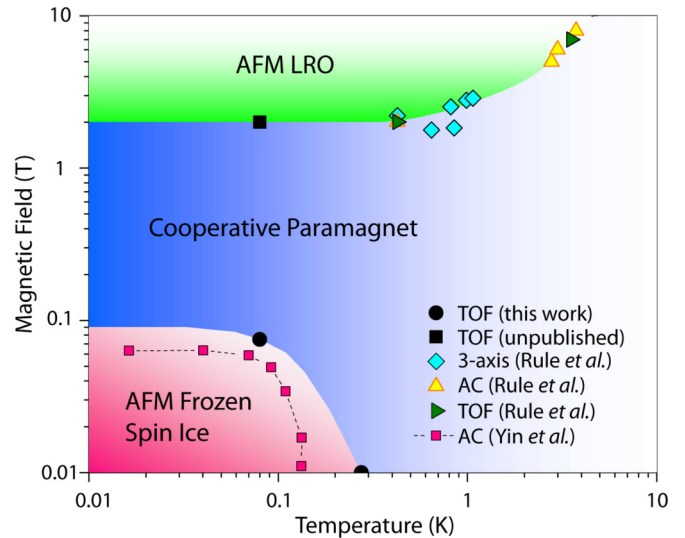
of frequency, to the frequency appropriate to our neutron measurements, ≈ 0.01 THz. Thus, a transition between 210 and 335 mK would be consistent with the range of previously reported ac-susceptibility peaks for different samples, which is in good agreement with our observations.

It is worth mentioning that the frozen behavior observed at low temperature in $Tb_2Ti_2O_7$ is not that of a canonical spin glass. Earlier μSR measurements revealed a slowing down of spin fluctuations upon cooling below 5 K, consistent with a freezing process, although the time dependence of the polarization clearly lacks the $\frac{1}{3}$ Kubo-Toyabe tail characteristic of static order, expected for canonical spin glasses such as CuMn [60]. Below 5 K, the spins remain largely dynamic as shown by the large spin-lattice relaxation rate and the field dependence of the relaxation. We also note that Lhotel *et al.* [38] report a distinction between the glassy behavior observed in $Tb_2Ti_2O_7$ and canonical spin glass behavior based on the frequency dependence of their ac-susceptibility data.

Based on the temperature and field dependence of the $(\frac{1}{2},\frac{1}{2},\frac{1}{2})$ elastic scattering, we can construct an H-T phase diagram for $Tb_2Ti_2O_7$ in the $[1\bar{1}0]$ field, shown in Fig. 5, including the high-field and high-temperature regions determined by Rule *et al.*'s work [45]. Note that both temperature and field axes are on a logarithmic scale. It is striking that our inelastic neutron scattering measurements and the ac-susceptibility work of Yin *et al.* [41] bound the same low-T, low-H phase in the phase diagram. Thus, we believe they pertain to the same microscopic origin, and demarcate the same frozen antiferromagnetic spin ice state deduced from the elastic neutron scattering pattern [37].

Higher energy resolution neutron scattering measurements with $E_i = 1.28$ meV were performed to investigate the
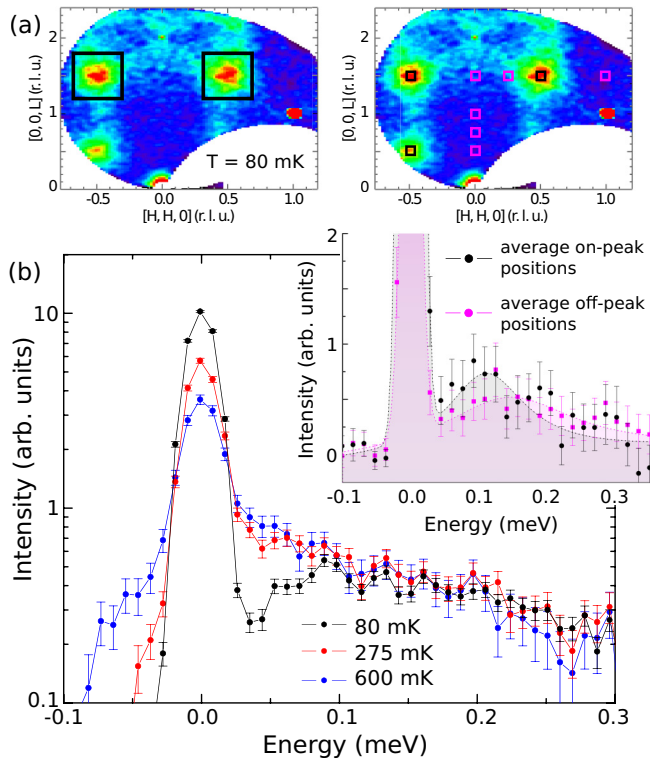
FIG. 6. (Color online) High-resolution inelastic neutron scattering data of $Tb_2Ti_2O_7$ in zero field. Panel (b) shows intensity vs energy transfer around the $(\frac{1}{2}, \frac{1}{2}, \frac{3}{2})$ and $(-\frac{1}{2}, -\frac{1}{2}, \frac{3}{2})$ positions, as a function of temperature. Note the logarithmic intensity scale. The **Q**-integration range (H = [±0.3, ± 0.7], L = [1.2,1.8] r.l.u.) is shown by the black squares in the scattering map on the left in panel (a). The inset to panel (b) shows the intensity vs energy transfer for the averaged $(\frac{1}{2}, \frac{1}{2}, \frac{1}{2})$ (on-peak) positions compared to other averaged (off-peak) positions at $T = 80$ mK. The shaded areas, bounded by phenomenological fits to a Gaussian (elastic line) and Lorentzian (inelastic) line shape for each of the on-peak and off-peak spectra, show a downwards shift of spectral weight by ≈ 0.05 meV at the $(\frac{1}{2}, \frac{1}{2}, \frac{1}{2})$ positions (gray color) compared to the off-peak (magenta) positions.

temperature and **Q** dependence of the low-lying spin excitations in $Tb_2Ti_2O_7$ in zero magnetic field. Figure 6(b) shows a plot of intensity vs energy transfer obtained by integrating over the two $(\frac{1}{2}, \frac{1}{2}, \frac{1}{2})$ positions in reciprocal space shown as the black squares in the left scattering map of Fig. 6(a). Data are shown for three different temperatures, in the ground state ($T = 80$ mK), near the spin-glass-like transition ($T = 275$ mK), and well above the transition ($T = 600$ mK). As the temperature is lowered through the transition at 275 mK, spectral weight is transferred from the low-energy inelastic channel into the resolution-limited elastic channel (-0.02 meV $< E <$ 0.02 meV), opening up a gap of ≈ 0.06 to 0.08 meV. The low-lying spin excitation spectrum above the gap extends at least up to ≈ 0.2 meV. This collapse of the magnetic spectral weight over much of the magnetic Brillouin zone into the elastic channel is a clear signature of spin freezing behavior, as observed in spin glasses such as $Y_2Mo_2O_7$ [61].

μSR measurements [16,55] in zero field have consistently reported persistent dynamics in the spin lattice relaxation rate down to very low temperatures in $Tb_2Ti_2O_7$, which may suggest that either the elastic scattering itself is not truly elastic on the lower frequency scale probed by μSR, or that the depletion of spectral weight in the spin gap is not complete.

Weak **Q** dependence is observed to the inelastic magnetic spectral weight at low temperatures, as shown in the inset to Fig. 6(b). This plot compares intensity vs energy transfer over small regions of reciprocal space centered on $\mathbf{Q}=(\frac{1}{2}, \frac{1}{2}, \frac{1}{2})$ wave vectors, and positions in reciprocal space far removed from $(\frac{1}{2}, \frac{1}{2}, \frac{1}{2})$ positions [referred to as "on-peak" and "off-peak" positions, which are shown in the black and magenta boxes, respectively, in the right panel of Fig. 6(a)]. The low-energy inelastic scattering appears to be gapped over the entire Brillouin zone, and the spectral weight extends slightly lower in energy at the $\mathbf{Q}=(\frac{1}{2}, \frac{1}{2}, \frac{1}{2})$ frozen antiferromagnetic spin ice zone center as compared with **Q** positions in the middle of the zone. While $Tb_2Ti_2O_7$ in zero field does not display conventional long-range order at any temperature and therefore does not exhibit well-defined spin wave excitations, this observation is consistent with a dispersion of a sort in the finite-lifetime spin excitations. These appear to soften somewhat at the $\mathbf{Q}=(\frac{1}{2}, \frac{1}{2}, \frac{1}{2})$ frozen antiferromagnetic spin ice zone center.

Taken together, our new neutron scattering data are fully consistent with a spin-glass-like transition near $T_g \approx 275$ mK in $H = 0$. This nonconventional spin glass state builds on short-range antiferromagnetic *spin ice* correlations, as opposed to either primarily short-range antiferromagnetic (e.g., $La_{2-x}Sr_xCuO_4$ [62]) or ferromagnetic correlations (e.g., $Eu_xSr_{1-x}S$ [63]), and has a low-temperature isotropic correlation length of ≈ 8 Å, as previously reported. The collapse of the low-energy magnetic spectral weight across the magnetic zone into short-range ordered elastic scattering at $\mathbf{Q}=(\frac{1}{2}, \frac{1}{2}, \frac{1}{2})$ wave vectors is a necessary component to this picture, informing on the magnetism in the frequency or time domain. It is also inconsistent with the singlet ground state scenario proposed theoretically for $Tb_2Ti_2O_7$ at low temperatures, since the inelastic magnetic intensity which forms the gap is transferred to elastic magnetic scattering, as opposed to being transferred above the gap leaving a nonmagnetic singlet ground state and an absence of elastic magnetic scattering. The magnetic spin glass ground state based on antiferromagnetic spin ice is also consistent with ac-susceptibility measurements which also show signatures for frozen, spin-glass-like ground states in a variety of $Tb_2Ti_2O_7$ samples, both in polycrystalline and single-crystal form. While there is some sample variation observed in the precise temperature at which a signature for a spin glass state is seen in $Tb_2Ti_2O_7$, all samples reported to date show such a signature in the approximate temperature range of 150–275 mK, consistent with the neutron scattering measurements we present in this work.

V. SPECIFIC HEAT

Significant sample variability has, however, been reported in anomalies, and the lack thereof, in the low temperature heat capacity measured on different samples of $Tb_2Ti_2O_7$ [31,44,54,55,64]. We note that sample variability in the position and sharpness of heat capacity anomalies at low
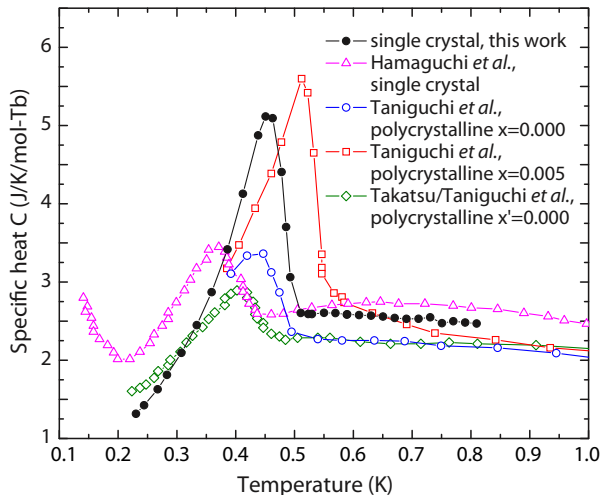
FIG. 7. (Color online) Specific heat versus temperature for different samples of $Tb_2Ti_2O_7$ in zero magnetic field. Measurements from a single crystal cut from the neutron scattering sample which we report on is shown in black. The clear anomaly at 450 mK does not coincide with the spin-glass-like transition at 275 mK indicated by our neutron scattering measurements. For comparison, we also show C_p data of other $Tb_2Ti_2O_7$ samples taken from the literature [44,54].

temperature in $Yb_2Ti_2O_7$ has also been reported [65], and this has been ascribed to the relative role of weak "stuffing" (excess Yb ions substituting on the Ti sublattice at the $\approx 2\%$ level). In particular, Taniguchi and co-workers studied a family of polycrystalline samples of the form $Tb_{2+x}Ti_{2-x}O_{7+y}$ for very small nonstoichiometry, $|x| < 0.005$. Such small levels of Tb excess/deficiency are difficult, if not impossible, to quantify *absolutely* using even the most sophisticated crystallographic techniques [65]. Taniguchi and co-workers have thus studied a series of polycrystalline $Tb_{2+x}Ti_{2-x}O_{7+y}$ samples with varying nominal x, which they found to be correlated with a systematic change in the lattice parameter. They report significant variability in both the temperature at which the heat capacity anomaly is observed, as well as in the amplitude of the anomaly. These anomalies in C_p are typically observed in the 400 mK to 500 mK regime in zero field. These results present two important questions for our study. First, does our neutron scattering single crystal sample of $Tb_2Ti_2O_7$ display such a C_p anomaly; if so how strong and at what temperature? Second, what is the relation between these sample-dependent C_p anomalies in zero field in $Tb_2Ti_2O_7$ and the transition to the frozen antiferromagnetic spin ice state we observe in our neutron scattering sample at $T_g \approx 275$ mK?

To address these questions we performed specific heat measurements down to a temperature of 220 mK on a 33.8 mg single crystal sample, cut from the same neutron scattering sample which was the focus of this paper and, as already mentioned, that of a previous study [45]. Figure 7 shows the measured specific heat of our single-crystal sample of $Tb_2Ti_2O_7$, compared with several other samples, both single crystals and polycrystals, taken from the literature [44,54]. As can be seen from Fig. 7, we observe a relatively large anomaly in C_p at ≈ 450 mK, almost twice the T_g associated

with the frozen antiferromagnetic spin ice state characterized in this paper with neutron scattering. For reference, we have indicated the location of the C_p anomaly in zero field in Fig. 3(c), which also shows the temperature dependence of the $\mathbf{Q} = (\frac{1}{2}, \frac{1}{2}, \frac{1}{2})$ elastic scattering. Clearly, the temperature scales associated with the results of these measurements are distinct. As this ≈ 450 mK temperature scale is not present in either our neutron scattering results or ac-susceptibility results on $Tb_2Ti_2O_7$ taken from the literature, we conclude that while this heat capacity anomaly and its associated sample dependence are intriguing and potentially important phenomena, they do not seem to originate from magnetic dipole degrees of freedom in $Tb_2Ti_2O_7$, similarly to what has recently been suggested in $Yb_2Ti_2O_7$ [66].

VI. CONCLUSION

In conclusion, our neutron scattering data on $Tb_2Ti_2O_7$ in a magnetic field show that a small field of ≈ 0.075 T applied along $[1\bar{1}0]$ is sufficient to destroy the short-range antiferromagnetically ordered spin ice state characterized by diffuse elastic scattering at $(\frac{1}{2}, \frac{1}{2}, \frac{1}{2})$ positions. This field range is consistent with phase boundary at $\mu_0 H_C \approx 0.067$ T for fields along [111] reported by Yin et al. [41], who also suggest that the zero-field ground state of $Tb_2Ti_2O_7$ is a quantum spin ice. The temperature dependence of the elastic diffuse scattering reveals a spin-glass-like freezing at $T_g \approx 275$ mK. The details of the neutron signatures associated with the $(\frac{1}{2}, \frac{1}{2}, \frac{1}{2})$ elastic scattering display some history dependence. The appearance of the elastic diffuse scattering below 275 mK correlates with the opening of a spin gap of 0.06–0.08 meV over most of reciprocal space and concomitant weakly dispersive spin excitations extending out to ≈ 0.2 meV. These excitations appear to soften at the short-range ordering positions of $(\frac{1}{2}, \frac{1}{2}, \frac{1}{2})$. Specific heat measurements on a piece of the same single crystal show an anomaly at 450 mK, consistent with other reports by Hamaguchi et al. and Taniguchi et al.. We observe no signs of an anomaly near 275 mK, indicating that different degrees of freedom are involved in the ordering process responsible for this specific heat anomaly in $Tb_2Ti_2O_7$. The new neutron measurements we report on the temperature and magnetic field parametrics allow us to complete the H-T magnetic phase diagram for $Tb_2Ti_2O_7$ in a $[1\bar{1}0]$ magnetic field. We find the dynamic and disordered, cooperative paramagnetic phase, which generated much of the original interest in $Tb_2Ti_2O_7$, to be bracketed by a low-field frozen antiferromagnetic spin ice state, and a field-induced, long-range ordered antiferromagnetic state at high fields.

[1] L. Balents, Nature (London) **464**, 199 (2010).

[2] S. B. Lee, S. Onoda, and L. Balents, Phys. Rev. B **86**, 104412 (2012).

[3] C. Lacroix, P. Mendels, and F. Mila, *Introduction to Frustrated Magnetism*, Springer Series in Solid-State Sciences (Springer, Heidelberg, 2011).

[4] T.-H. Han, J. S. Helton, S. Chu, D. G. Nocera, J. A. Rodriguez-Rivera, C. Broholm, and Y. S. Lee, Nature (London) **492**, 406 (2012).

[5] J. S. Helton, K. Matan, M. P. Shores, E. A. Nytko, B. M. Bartlett, Y. Yoshida, Y. Takano, A. Suslov, Y. Qiu, J.-H. Chung, D. G. Nocera, and Y. S. Lee, Phys. Rev. Lett. **98**, 107204 (2007).

[6] P. Mendels, F. Bert, M. A. de Vries, A. Olariu, A. Harrison, F. Duc, J. C. Trombe, J. S. Lord, A. Amato, and C. Baines, Phys. Rev. Lett. **98**, 077204 (2007).

[7] Y. Shimizu, K. Miyagawa, K. Kanoda, M. Maesato, and G. Saito, Phys. Rev. Lett. **91**, 107001 (2003).

[8] F. L. Pratt, P. J. Baker, S. J. Blundell, T. Lancaster, S. Ohira-Kawamura, C. Baines, Y. Shimizu, K. Kanoda, I. Watanabe, and G. Saito, Nature (London) **471**, 612 (2011).

[9] J. S. Gardner, M. J. P. Gingras, and J. E. Greedan, Rev. Mod. Phys. **82**, 53 (2010).

[10] S. T. Bramwell and M. J. P. Gingras, Science **294**, 1495 (2001).

[11] C. Castelnovo, R. Moessner, and S. Sondhi, Annu. Rev. Condens. Matter Phys. **3**, 35 (2012).

[12] L. Savary, K. A. Ross, B. D. Gaulin, J. P. C. Ruff, and L. Balents, Phys. Rev. Lett. **109**, 167201 (2012).

[13] K. A. Ross, L. Savary, B. D. Gaulin, and L. Balents, Phys. Rev. X **1**, 021002 (2011).

[14] T. Fennell, P. P. Deen, A. R. Wildes, K. Schmalzl, D. Prabhakaran, A. T. Boothroyd, R. J. Aldus, D. F. McMorrow, and S. T. Bramwell, Science **326**, 415 (2009).

[15] D. J. P. Morris, D. A. Tennant, S. A. Grigera, B. Klemke, C. Castelnovo, R. Moessner, C. Czternasty, M. Meissner, K. C. Rule, J.-U. Hoffmann, K. Kiefer, S. Gerischer, D. Slobinsky, and R. S. Perry, Science **326**, 411 (2009).

[16] J. S. Gardner, S. R. Dunsiger, B. D. Gaulin, M. J. P. Gingras, J. E. Greedan, R. F. Kiefl, M. D. Lumsden, W. A. MacFarlane, N. P. Raju, J. E. Sonier, I. Swainson, and Z. Tun, Phys. Rev. Lett. **82**, 1012 (1999).

[17] M. J. P. Gingras, B. C. den Hertog, M. Faucher, J. S. Gardner, S. R. Dunsiger, L. J. Chang, B. D. Gaulin, N. P. Raju, and J. E. Greedan, Phys. Rev. B **62**, 6496 (2000).

[18] I. Mirebeau, P. Bonville, and M. Hennion, Phys. Rev. B **76**, 184436 (2007).

[19] J. Zhang, K. Fritsch, Z. Hao, B. V. Bagheri, M. J. P. Gingras, G. E. Granroth, P. Jiramongkolchai, R. J. Cava, and B. D. Gaulin, Phys. Rev. B **89**, 134410 (2014).

[20] B. C. den Hertog and M. J. P. Gingras, Phys. Rev. Lett. **84**, 3430 (2000).

[21] J. S. Gardner, A. Keren, G. Ehlers, C. Stock, E. Segal, J. M. Roper, B. Fåk, M. B. Stone, P. R. Hammar, D. H. Reich, and B. D. Gaulin, Phys. Rev. B **68**, 180401 (2003).

[22] H. R. Molavian, M. J. P. Gingras, and B. Canals, Phys. Rev. Lett. **98**, 157204 (2007).

[23] H. R. Molavian, P. A. McClarty, and M. J. P. Gingras, arXiv:0912.2957.

[24] B. D. Gaulin, J. S. Gardner, P. A. McClarty, and M. J. P. Gingras, Phys. Rev. B **84**, 140402 (2011).

[25] P. Bonville, S. Petit, I. Mirebeau, J. Robert, E. Lhotel, and C. Paulsen, arXiv:1302.6418.

[26] H. R. Molavian and M. J. P. Gingras, J. Phys.: Condens. Matter **21**, 172201 (2009).

[27] P. Bonville, I. Mirebeau, A. Gukasov, S. Petit, and J. Robert, Phys. Rev. B **84**, 184409 (2011).

[28] O. Benton, O. Sikora, and N. Shannon, Phys. Rev. B **86**, 075154 (2012).

[29] J. P. C. Ruff, B. D. Gaulin, J. P. Castellan, K. C. Rule, J. P. Clancy, J. Rodriguez, and H. A. Dabkowska, Phys. Rev. Lett. **99**, 237202 (2007).

[30] J. P. C. Ruff, Z. Islam, J. P. Clancy, K. A. Ross, H. Nojiri, Y. H. Matsuda, H. A. Dabkowska, A. D. Dabkowski, and B. D. Gaulin, Phys. Rev. Lett. **105**, 077203 (2010).

[31] T. Fennell, M. Kenzelmann, B. Roessli, H. Mutka, J. Ollivier, M. Ruminy, U. Stuhr, O. Zaharko, L. Bovo, A. Cervellino, M. K. Haas, and R. J. Cava, Phys. Rev. Lett. **112**, 017203 (2014).

[32] S. Guitteny, J. Robert, P. Bonville, J. Ollivier, C. Decorse, P. Steffens, M. Boehm, H. Mutka, I. Mirebeau, and S. Petit, Phys. Rev. Lett. **111**, 087201 (2013).

[33] I. V. Aleksandrov, B. V. Lidskii, L. G. Mamsurova, M. G. Neigauz, K. S. Pigal'skii, K. K. Pukhov, N. G. Trusevich, and L. G. Shcherbakova, Sov. Phys. JETP **62**, 1287 (1985).

[34] L. G. Mamsurova, K. S. Pigal'skii, and K. K. Pukhov, JETP Lett. **43**, 755 (1986).

[35] T. Fennell, M. Kenzelmann, B. Roessli, M. K. Haas, and R. J. Cava, Phys. Rev. Lett. **109**, 017201 (2012).

[36] S. Petit, P. Bonville, J. Robert, C. Decorse, and I. Mirebeau, Phys. Rev. B **86**, 174403 (2012).

[37] K. Fritsch, K. A. Ross, Y. Qiu, J. R. D. Copley, T. Guidi, R. I. Bewley, H. A. Dabkowska, and B. D. Gaulin, Phys. Rev. B **87**, 094410 (2013).

[38] E. Lhotel, C. Paulsen, P. D. de Réotier, A. Yaouanc, C. Marin, and S. Vanishri, Phys. Rev. B **86**, 020410 (2012).

[39] P. J. Baker, M. J. Matthews, S. R. Giblin, P. Schiffer, C. Baines, and D. Prabhakaran, Phys. Rev. B **86**, 094424 (2012).

[40] S. Legl, C. Krey, S. R. Dunsiger, H. A. Dabkowska, J. A. Rodriguez, G. M. Luke, and C. Pfleiderer, Phys. Rev. Lett. **109**, 047201 (2012).

[41] L. Yin, J. S. Xia, Y. Takano, N. S. Sullivan, Q. J. Li, and X. F. Sun, Phys. Rev. Lett. **110**, 137201 (2013).

[42] A. P. Sazonov, A. Gukasov, H. B. Cao, P. Bonville, E. Ressouche, C. Decorse, and I. Mirebeau, Phys. Rev. B **88**, 184428 (2013).

[43] R. Higashinaka (private communication).

[44] T. Taniguchi, H. Kadowaki, H. Takatsu, B. Fåk, J. Ollivier, T. Yamazaki, T. J. Sato, H. Yoshizawa, Y. Shimura, T. Sakakibara, T. Hong, K. Goto, L. R. Yaraskavitch, and J. B. Kycia, Phys. Rev. B **87**, 060408 (2013).

[45] K. C. Rule, J. P. C. Ruff, B. D. Gaulin, S. R. Dunsiger, J. S. Gardner, J. P. Clancy, M. J. Lewis, H. A. Dabkowska, I. Mirebeau, P. Manuel, Y. Qiu, and J. R. D. Copley, Phys. Rev. Lett. **96**, 177201 (2006).

[46] H. A. Dabkowska and A. B. Dabkowski, in *Springer Handbook of Crystal Growth*, edited by G. Dhanaraj (Springer, Berlin, 2010), pp. 367–392.

[47] J. Gardner, B. Gaulin, and D. McK Paul, J. Cryst. Growth **191**, 740 (1998).

[48] J. R. D. Copley and J. C. Cook, Chem. Phys. **292**, 477 (2003).

[49] K. A. Ross, J. P. C. Ruff, C. P. Adams, J. S. Gardner, H. A. Dabkowska, Y. Qiu, J. R. D. Copley, and B. D. Gaulin, Phys. Rev. Lett. **103**, 227202 (2009).

[50] R. Applegate, N. R. Hayre, R. R. P. Singh, T. Lin, A. G. R. Day, and M. J. P. Gingras, Phys. Rev. Lett. **109**, 097205 (2012).

[51] N. R. Hayre, K. A. Ross, R. Applegate, T. Lin, R. R. P. Singh, B. D. Gaulin, and M. J. P. Gingras, Phys. Rev. B **87**, 184423 (2013).

[52] S. H. Curnoe, Phys. Rev. B **88**, 014429 (2013).

[53] P. Bonville, A. Gukasov, I. Mirebeau, and S. Petit, Phys. Rev. B **89**, 085115 (2014).

[54] N. Hamaguchi, T. Matsushita, N. Wada, Y. Yasui, and M. Sato, Phys. Rev. B **69**, 132413 (2004).

[55] A. Yaouanc, P. Dalmas de Réotier, Y. Chapuis, C. Marin, S. Vanishri, D. Aoki, B. Fåk, L.-P. Regnault, C. Buisson, A. Amato, C. Baines, and A. D. Hillier, Phys. Rev. B **84**, 184403 (2011).

[56] J. A. Mydosh, *Spin Glasses: An Experimental Introduction* (CRC Press, Bristol, PA, 1993).

[57] K. Binder and A. P. Young, Rev. Mod. Phys. **58**, 801 (1986).

[58] P. Schiffer group (private communication).

[59] G. Luo, S. T. Hess, and L. Corruccini, Phys. Lett. A **291**, 306 (2001).

[60] Y. J. Uemura, T. Yamazaki, D. R. Harshman, M. Senba, and E. J. Ansaldo, Phys. Rev. B **31**, 546 (1985).

[61] J. S. Gardner, B. D. Gaulin, S.-H. Lee, C. Broholm, N. P. Raju, and J. E. Greedan, Phys. Rev. Lett. **83**, 211 (1999).

[62] M. Fujita, K. Yamada, H. Hiraka, P. Gehring, S. Lee, S. Wakimoto, and G. Shirane, Phys. Rev. B **65**, 064505 (2002).

[63] H. Maletta, G. Aeppli, and S. Shapiro, J. Magn. Magn. Mater. **31–34**, 1367 (1983).

[64] Y. Chapuis, Ph.D. thesis, Université Joseph Fourier, 2009.

[65] K. A. Ross, T. Proffen, H. A. Dabkowska, J. A. Quilliam, L. R. Yaraskavitch, J. B. Kycia, and B. D. Gaulin, Phys. Rev. B **86**, 174424 (2012).

[66] R. M. D'Ortenzio, H. A. Dabkowska, S. R. Dunsiger, B. D. Gaulin, M. J. P. Gingras, T. Goko, J. B. Kycia, L. Liu, T. Medina, T. J. Munsie, D. Pomaranksi, K. A. Ross, Y. J. Uemura, T. J. Williams, and G. M. Luke, Phys. Rev. B **88**, 134428 (2013).

[67] R. T. Azuah, L. R. Kneller, Y. Qiu, P. L. W. Tregenna-Piggott, C. M. Brown, J. R. D. Copley, and R. M. Dimeo, J. Res. Natl. Inst. Stand. Technol. **114**, 341 (2009).